New Phytologist

Research

The hidden diversity of vascular patterns in flower heads

Andrew Owens[1]*, Teng Zhang[2]*, Philmo Gu[1], Jeremy Hart[1], Jarvis Stobbs[3], Mikolaj Cieslak[1], Paula Elomaa[2] and Przemyslaw Prusinkiewicz[1]

[1]Department of Computer Science, University of Calgary, Calgary, AB, T2N 1N4, Canada; [2]Department of Agricultural Sciences, Viikki Plant Science Centre, University of Helsinki, PO Box 27, Helsinki, 00014, Finland; [3]Canadian Light Source Inc., 44 Innovation Blvd, Saskatoon, SK, S7N 2V3, Canada

Authors for correspondence:
Mikolaj Cieslak
Email: msciesla@ucalgary.ca

Paula Elomaa
Email: paula.elomaa@helsinki.fi

Przemyslaw Prusinkiewicz
Email: pwp@ucalgary.ca

Received: *11 November 2023*
Accepted: *18 January 2024*

New Phytologist (2024)
doi: 10.1111/nph.19571

Key words: Asteraceae, computational modeling, phyllotaxis, reticulation, sectoriality, synchrotron X-ray micro-CT, vascular architecture, visualization.

Summary

- Vascular systems are intimately related to the shape and spatial arrangement of the plant organs they support. We investigate the largely unexplored association between spiral phyllotaxis and the vascular system in Asteraceae flower heads.
- We imaged heads of eight species using synchrotron-based X-ray micro-computed tomography and applied original virtual reality and haptic software to explore head vasculature in three dimensions. We then constructed a computational model to infer a plausible patterning mechanism.
- The vascular system in the head of the model plant *Gerbera hybrida* is qualitatively different from those of *Bellis perennis* and *Helianthus annuus*, characterized previously. *Cirsium vulgare*, *Craspedia globosa*, *Echinacea purpurea*, *Echinops bannaticus*, and *Tanacetum vulgare* represent variants of the Bellis and Helianthus systems. In each species, the layout of the main strands is stereotypical, but details vary. The observed vascular patterns can be generated by a common computational model with different parameter values.
- In spite of the observed differences of vascular systems in heads, they may be produced by a conserved mechanism. The diversity and irregularities of vasculature stand in contrast with the relative uniformity and regularity of phyllotactic patterns, confirming that phyllotaxis in heads is not driven by the vasculature.

Introduction

The development of vascular tissues is one of the key evolutionary innovations that resulted in the explosive radiation of plants on Earth. Vascular tissues, composed of xylem and phloem, provide mechanical support for plants as well as a route for the transport of water, nutrients and signaling molecules such as hormones (Lucas *et al.*, 2013). The vascular system extends throughout an entire plant (Esau, 1965a,b). At the level of individual organs, leaf venation patterns have received much attention due to their complexity, diversity, and easy accessibility to direct observation. At the whole-plant level, studies have focused on vasculature in roots and shoot stems.

Until recently, the analysis of volumetric vascular structures involved the laborious process of obtaining serial tissue sections and inferring the three-dimensional structure of the vascular system from them (Kaplan, 1937; Kang *et al.*, 2003). Computed tomography (CT) alleviates this methodological difficulty by directly providing three-dimensional data stacks (Stuppy *et al.*, 2003; Lee *et al.*, 2006). In this paper, we employ laboratory- and synchrotron-radiation-based X-ray micro-computed tomography (Withers *et al.*, 2021) complemented with computational modeling to investigate the vascular patterns of flower heads. While micro-CT has been found useful for studying internal plant structures (e.g. Dhondt *et al.*, 2010; Karunakaran *et al.*, 2015; Prunet & Duncan, 2020; Piovesan *et al.*, 2021) including stem vasculature (Brodersen *et al.*, 2011, 2012; McElrone *et al.*, 2013; Brodersen & Roddy, 2016), the imaging and analysis of flower heads represent a particular challenge due to the geometric complexity of their vascular systems.

Flower heads – the inflorescences in the Asteraceae plant family – typically consist of hundreds of small, densely packed florets attached to an enlarged receptacle and surrounded by protective involucral bracts. The involucral bracts and florets are arranged into intersecting left- and right-winding spirals (parastichies), which frequently occur in consecutive Fibonacci numbers (Jean, 1994; Barabé & Lacroix, 2020). The geometric regularity and mathematical properties of these patterns have attracted multidisciplinary interest for centuries (Adler *et al.*, 1997). They have also raised questions regarding the organization of the vascular system that supplies the florets with water and nutrients. Historically first, Philipson (1946) reported that the primary vascular strands in the heads of *Bellis perennis* (common daisy) formed a reticulate network aligned with the parastichies, that is with the main vascular strands parallel to the spiral phyllotactic arrangement of the florets. Subsequently, Philipson (1948) reported a similar pattern in two other members of the Aster family: *Hieracium boreale* and *Dahlia gracilis*. By contrast, Durrieu *et al.* (1985)

*Co-first authors.

found that the vascular network in the heads of *Helianthus annuus* (common sunflower) was organized sectorially, with the main vascular strands spreading radially from the stem toward the head rim, and the veins from involucral bracts and florets attaching to these strands irrespective of the parastichy pattern. The sectorial organization of the sunflower head vasculature was confirmed by Alkio *et al.* (2002), who demonstrated that photoassimilates tagged with radioactive carbon propagated to achenes (seeds) along radial sectors, as opposed to following the parastichy pattern.

The discrepancy between the vasculature of Bellis and sunflower heads raised our interest in the type of vasculature present in *Gerbera hybrida*, a model plant used to study the phyllotaxis of heads (Zhang *et al.*, 2021). Using synchrotron-radiation-based X-ray micro-computed tomography (SR-μCT) imaging, we show that gerbera head vasculature is also organized sectorially, but its organization is qualitatively different from that of the sunflower heads reported by Durrieu. To exclude the possibility that this discrepancy is due to different experimental methods, we also applied SR-μCT to image sunflower and Bellis heads. Our results confirmed those reported previously while augmenting Philipson's description of Bellis with more detailed observations. Intrigued by the differences between gerbera, sunflower, and Bellis, we have additionally imaged the heads of five previously unstudied species: *Cirsium vulgare* (common thistle), *Craspedia globosa*, *Echinacea purpurea* (coneflower), *Echinops bannaticus*, and *Tanacetum vulgare*. We show that their vascular systems are variants of, or intermediate between, those observed in Bellis and sunflower.

The observed complexity and diversity of vascular patterns in heads lead to the question of how these patterns develop. Data (Zhang *et al.*, 2021) suggest that the basic patterning processes in heads are similar to those found in the inflorescences of plants not forming heads, such as Arabidopsis (Reinhardt *et al.*, 2003), tomato (Bayer *et al.*, 2009), and *Brachypodium* (O'Connor *et al.*, 2014). The key patterning mechanism is the interaction between the plant hormone auxin and its cellular transporters, primarily the PIN1 efflux carriers. It leads to the emergence of auxin concentration maxima that organize the incipient primordia into a phyllotactic pattern, and canals of auxin transport that connect these primordia to the already formed vasculature, patterning new strands. These processes are best understood with the help of computational models (Prusinkiewicz & Runions, 2012). However, the existing models that simulate vascular patterns directly at the level of molecular interactions only capture relatively simple patterns and pattern elements, such as canals connecting auxin sources to sinks, and operate on two-dimensional leaf blades or plant sections (Runions *et al.*, 2014). To overcome this limitation and capture the complex three-dimensional vascular architecture of flower heads, we present a higher level model in which molecular interactions are distilled into geometric rules.

Materials and Methods

Plant material

Gerbera hybrida (*G. jamesonii* Bolus ex Adlam × *G. viridifolia* Schultz-Bip.) cv Terra Regina, the transgenic gerbera lines expressing the constructs for the antisense-*GRCD2* line TR15 (Uimari *et al.*, 2004; Zhang *et al.*, 2017), the *DR5rev:3xVENUS-N7* line TR3 (Zhang *et al.*, 2021), as well as *H. annuus* L. cv Pacino cola and *C. globosa* (F.L. Bauer ex Benth.) Benth. plants were grown under standard glasshouse conditions. Samples from *B. perennis* L., *E. purpurea* (L.) Moench cv White Swan, *E. bannaticus* Rochel ex Schrad, *T. vulgare* L. and *C. vulgare* (Savi) Ten. plants were collected from outdoor grown plants in Helsinki, Finland. For each species, fully patterned flower heads were collected in two biological replicates. In addition to the developmental series of gerbera head samples collected previously (Zhang *et al.*, 2021), sample series were collected for sunflower and Bellis. After discarding similar samples, 10 of 20 gerbera samples, nine of 13 sunflower samples, and seven of 33 Bellis samples were selected for further analysis. The smallest samples with embedded early-stage head meristems (diameter < 1 mm) were randomly dissected from the plants under a stereomicroscope, and the developmental stage of the meristems was estimated on the basis of the micro-CT imaging. Following the collection, the samples were fixed, dehydrated, critical-point dried, and mounted on scanning electron microscopy (SEM) stubs as described by Zhang *et al.* (2021).

Micro-computed tomography

Head samples were scanned using laboratory-based or SR-based X-ray micro-CT. The choice of the technique was affected by its availability and technological progress over the duration of our study (2016–2022), with a preference for SR-μCT due to the superior quality of the resulting images. The laboratory-based scanners were a Skyscan 1272 micro-CT scanner (Bruker Corporation, Billerica, MA, USA) and a GE Phoenix Nanotom scanner (GE Sensing & Inspection Technologies GmbH, Wunstorf, Germany). Synchrotron scanning was conducted at the Biomedical Imaging and Therapy (BMIT) facility at the Canadian Light Source, Saskatoon, Canada, https://bmit.lightsource.ca. We used the bending magnet beamline (05B1-1) with the X-ray energy of *c.* 20 kV, which had been found optimal for imaging plant samples (Karunakaran *et al.*, 2015). The beamline produces a monochromatic and partially coherent beam, which we employed to enhance contrast using phase-contrast imaging. Details concerning the synchrotron scanning are given in the Supporting Information Methods S1, and attributes pertinent to the scanning and visualization of individual heads are listed in Table S1.

Tomographic image reconstruction

Three-dimensional image stacks were reconstructed from the projection images using NRecon v.1.7.0.1 (Bruker Micro-CT) or the Tofu image processing toolkit (Faragó *et al.*, 2022) included in the ufo-kit 0.9 package (Vogelgesang *et al.*, 2016) augmented with the EZ-UFO graphical interface (https://github.com/sgasilov/ez_ufo, S. Gazilov, Canadian Light Source), using default configuration parameters. The methods applied to the specific samples are indicated in Table S1. Ring artefacts in the tomograms were suppressed using a low-pass Gaussian filter. Multiple sections of tall samples were combined into one image

stack using ImageJ/Fiji (Schindelin *et al.*, 2012), by visually matching scans in the overlapping portions of each section. To reduce file sizes, each image stack was cropped to eliminate excessive background and reduced from 32-bit to 16-bit representation by selecting the relevant portion of the histogram using ImageJ/Fiji. The final stacks were assembled into tiff (Tag Image File Format) files. The reconstructions were carried out using Dell Alienware Area-51 Desktop PC with a 3.1 GHz Intel Core i9-7940X CPU, 64 GB RAM, and a NVIDIA GeForce RTX 2080 Ti graphics card with 11 GB VRAM, running the Windows 10 Enterprise operating system (NRecon reconstructions) or Linux Ubuntu 18.04 (UFO-KIT reconstructions).

3D image analysis, segmentation, and visualization

The reconstructed image stacks were analyzed using ImageJ/Fiji, MorphographX (Barbier de Reuille *et al.*, 2015), and two experimental programs, SHVR (Gu, 2022) and ViNE (Hart, 2020), developed at the University of Calgary (https://github.com/AlgorithmicBotany). SHVR operates directly on volumetric data and facilitates segmentation of vascular strands by using a haptic device (3D Systems Touch, Rock Hill, SC, USA) to give the operator the impression of physically touching and following them. ViNE operates on polygonal meshes extracted from volumetric data and facilitates segmentation by using a virtual reality system, which gives the operator the impression of being immersed in the flower head and segmenting vascular strands directly in 3D. The isosurface meshes were generated using a custom-made IsoPoly program utilizing the OpenVDB library (https://www.openvdb.org). The final images were rendered directly by SHVR or ViNE, or were output as PLY (Polygon File Format) files and rendered using Blender v.2.8 (https://blender.org). Videos were assembled using FFmpeg (https://www.ffmpeg.org). While diverse hardware was used for software development and research, the results have been tested and are reproducible on the Dell Alienware desktop PC running Windows 10 Enterprise (as specified above) coupled with the 3D Systems Touch haptic device (for SHVR) or the HTC Corporation (New Taipei, Taiwan) Vive virtual reality system (for ViNE).

Histological analysis

To obtain additional information of the early stages of head development, we complemented tomographic imaging with histological analysis. Five rosette sectors containing representative head meristems were collected from the transgenic gerbera plants expressing the *DR5rev:3xVENUS-N7* auxin reporter construct (Zhang *et al.*, 2021). To visualize the DR5 signals, the samples were first imaged with a Leica FCA M205 fluorescence stereomicroscope (Leica Microsystems, Wetzlar, Germany) using a GFP filter. The same samples were then fixed, dehydrated, and embedded in paraffin blocks as described by Laitinen *et al.* (2006). Serial 10-μm sections were cut in a horizontal direction using a microtome. The paraffin strips were attached to imaging slides, deparaffinized and stained in 0.2% toluidine blue for 10 min. After washing with sterile H_2O for three times, the slides were mounted with 50% glycerol and imaged with a Leica FCA M205 microscope.

Computational modeling

To investigate the mechanism of vascular patterning in flower heads and the causes of their diversity, we constructed parametrized simulation models of vascular patterning in gerbera, sunflower, and Bellis. Vascular patterning was simulated on data-driven models of growing heads with simulated phyllotactic patterns. For gerbera, we used the flower head model of Zhang *et al.* (2021); for sunflower and Bellis, we recalibrated that model using image data obtained by scanning the respective heads at different developmental stages. All models were written in C++ extended with constructs of the L+C plant modeling language (Karwowski & Prusinkiewicz, 2003; Prusinkiewicz *et al.*, 2007), and executed using the lpfg simulator incorporated into the Virtual Laboratory (vlab) v.5.0 plant modeling environment (http://algorithmicbotany.org or https://github.com/AlgorithmicBotany). Simulations were performed on MacBook Pro computers under macOS High Sierra. Videos were assembled using FFmpeg.

Results

Gerbera flower head displays a previously undescribed sectorial vascular system

A gerbera (cv Terra Regina) head has *c.* 600–700 individual florets surrounded by 80–90 involucral bracts (Zhang *et al.*, 2021) (Fig. 1a,b; for all morphological features, see also Video S1). The bracts and florets form on a mushroom-shaped receptacle with a convex but relatively flat upper (adaxial) surface that meets the lower (abaxial) surface along a discernible rim (Fig. 1c, dashed white line). Synchrotron-radiation-based X-ray micro-computed tomography imaging revealed that the stem supporting the head has *c.* 30 longitudinal vascular strands (Fig. S1d,e). Upon entering the receptacle, these strands branch and spread radially toward the receptacle rim (Figs 1d, S1d,e), and occasionally merge. The outermost strands enter the involucral bracts, where they split into parallel veins running the length of each bract. The intermediate strands, enter ray and trans florets near the head rim. The innermost strands change direction and extend toward the receptacle center, forming a system of adaxial strands (Figs 1c, 2b,c, S1b,c). Approaching the head center, some of these strands terminate early or merge, such that their density remains approximately constant (Fig. 2b). Individual disc florets connect with the adaxial strands via one or several floret veins, which are approximately perpendicular to the upper surface of the receptacle (Fig. 2b,c). Except close to the rim, the ground tissue (parenchyma) of the receptacle does not contain discernible vasculature (Fig. 1c).

We further analyzed the connections between vascular strands and florets by segmenting florets connected to selected adaxial strands using the ViNE software (Fig. 2d,e). Our analysis confirmed that the vascular system of the gerbera heads is organized sectorially, as implied by the radial organization of the main abaxial and adaxial strands (Figs 1c,d, 2b,c). This organization is independent of the spiral phyllotaxis of the head: An individual adaxial strand supplies floret primordia that belong to different

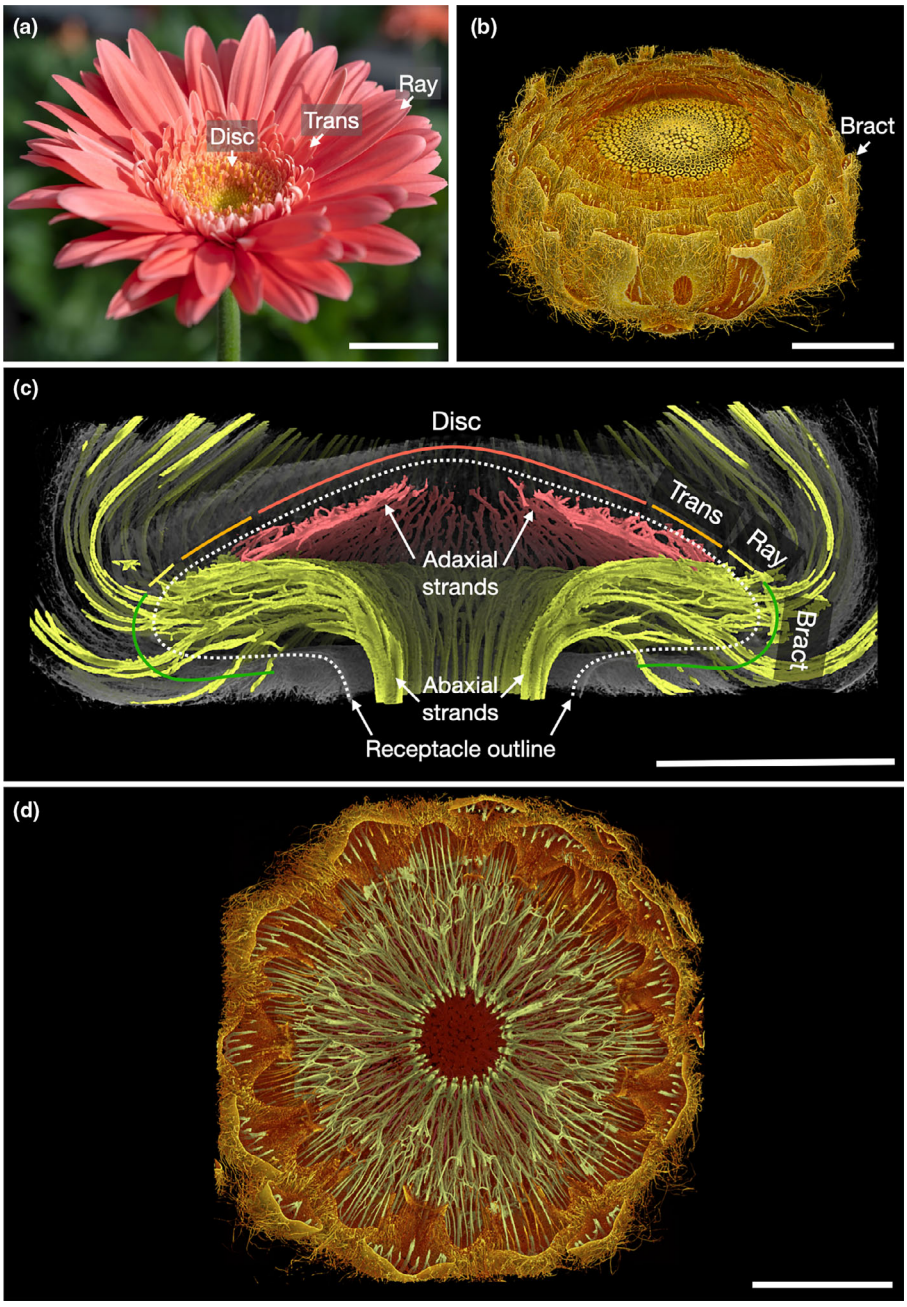

Fig. 1 Vascular architecture of gerbera heads. (a) A mature head with three different types of florets (ray, trans, disc) emerging acropetally from the margin of the head. (b) 3D reconstruction of an earlier developmental stage of a gerbera flower head. (c) Longitudinal side view of half of the head with the vascular system segmented using SHVR. The abaxial and adaxial vascular strands are colored green and red, respectively. (d) A virtual transverse cut showing the abaxial vascular system within a gerbera head. The branched vascular system spreads from the stem radially and enters the involucral bracts at the head rim. Bars: (a) 2 cm; (b–d) 5 mm.

parastichies, while florets that belong to different segments of the same parastichy are supplied by different adaxial strands (Fig. 2d,e).

3D visualization confirms previously described vascular patterns in Bellis and sunflower

Our analysis indicated that the vascular network in gerbera is qualitatively different from those previously reported in Bellis (Philipson, 1946) and sunflower (Durrieu *et al.*, 1985). To confirm that the observed differences are not an artefact of distinct experimental methods, we have imaged, segmented, and analyzed Bellis and sunflower heads using SR-μCT as well (Fig. 3). As in gerbera, the florets in these species are arranged into spiral phyllotactic patterns (Fig. 3a,e), although the receptacles have different overall shapes. The receptacle in sunflower (cv Pacino cola) is concave with a shallow, slightly depressed central region, which raises toward the peripheral rim (Fig. 3c). By contrast, the receptacle of Bellis is a vertically elongated dome (Fig. 3g).

Our observations were consistent with those reported previously. As in gerbera, the vasculature of sunflower heads is organized sectorially, with no correspondence between abaxial strands and the phyllotactic pattern (Fig. S2b,c). Large abaxial strands spread outward from the stem to the involucral bracts and peripheral ray florets (Figs 3c,d, S2a,b) but, in contrast to gerbera, there are no adaxial strands extending inward: The floret veins

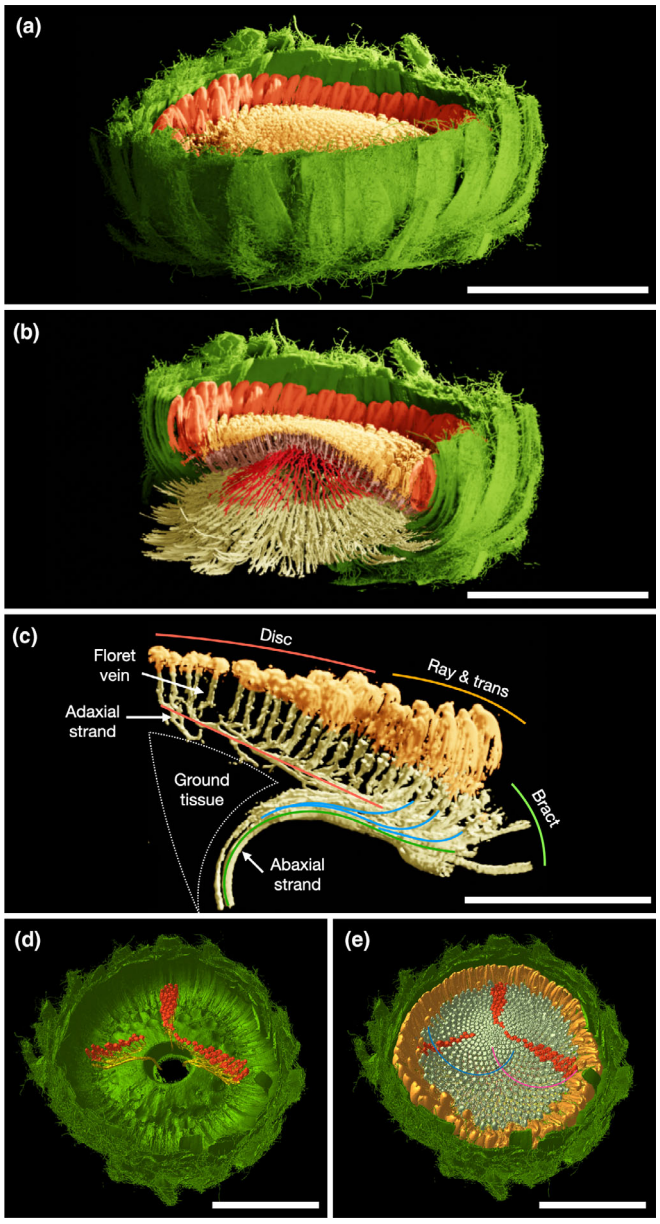

Fig. 2 Phyllotaxis and the vascular system in a gerbera flower head. (a) 3D rendering of a scanned gerbera head segmented using VINE, indicating the bracts (green), ray florets (orange), and disc florets (yellow). (b) A virtual cut exposing the vascular structure of the same head. Abaxial strands (straw-colored) extend outward to the bracts and connect near the head perimeter to adaxial strands (red), which extend towards the head center. Short floret veins (purple), perpendicular to the receptacle surface, connect florets to the adaxial veins. (c) An isolated sector of the vascular system showing adaxial strands (highlighted in red) originating from a single abaxial strand, and the connected floret veins. The abaxial strands connect to bracts (green), and ray and trans florets (blue). (d) A flower head from above with all but three vascular strands emerging from the stem removed. The vascular system originating from each strand (yellow) supports a separate sector of florets on the head (red). (e) The same flower head as (d) with all florets displayed, showing that the florets in each sector are from different parastichies. A representative pair of spiral parastichies are highlighted with blue and pink lines. Bars: (a, b, d, e) 1 cm; (c) 5 mm.

connect directly to the abaxial strands across the parenchyma (Fig. 3d). As observed by Durrieu *et al.* (1985), the course of these veins is highly irregular and they often merge, forming a branched system (Fig. 3d).

Likewise, our observations of the vasculature of Bellis generally agree with those of Philipson (1946). The Bellis head vasculature forms a regular reticulate network of vascular strands aligned with the parastichies (Figs 3g, S3a,b). However, using SR-μCT, we observed more details. Individual floret veins attach to this network near, but not always exactly at, the point of intersection between opposite parastichies (Fig. S3c,d). This regularity breaks near the base of the head, where strands from the stem enter the receptacle and form a less reticulated network. Connections corresponding to one of the two intersecting parastichies are often missing, producing gaps at the base of the network (Fig. 3h, yellow lines).

In summary, the vascular system in gerbera heads exhibits a previously unobserved type of architecture. In addition, our data confirm the previously reported qualitative differences between the vascular systems of Bellis (Philipson, 1946) and sunflower (Durrieu *et al.*, 1985) and provide additional insights into their three-dimensional structure.

Vascular patterns in other observed heads are intermediate between sunflower and Bellis

Having observed that flower heads of the three analyzed species have qualitatively different vascular networks, we inquired whether this diversity extends to other Asteraceae species. We analyzed five additional species, resulting in a total of eight species representing two distinct subfamilies of Asteraceae: Cichorioideae (gerbera, thistle and Echinops) and Asteroideae (sunflower, Bellis, coneflower, Tanacetum, and Craspedia) (Figs 4, S4). None of the additionally scanned species had a vascular system identical to any of the original three species. However, each system could be interpreted as a combination of features from sunflower and Bellis.

The receptacle of thistle heads (Fig. 4a–c) is conical. Similar to the sunflower, the floret veins connect directly to the abaxial stem strands (Fig. 4c) and are organized sectorially (Fig. S4a,b). The vascular strands entering the head from the stem extend along the bristly abaxial side of the receptacle and occasionally interconnect (Fig. 4c). These interconnections relate thistle vasculature to Bellis.

Coneflower (Fig. 4d–f) also develops a conical receptacle (Bremer, 1994) and, similar to thistle, has floret veins organized sectorially (Figs 4f, S4c, top). In contrast to sunflower and thistle, these veins do not self-organize into highly branched structures deeply penetrating the parenchyma (Fig. 3d), but form meandering strands that extend from the head periphery toward the center while remaining close to the adaxial surface of the receptacle (Fig. 4f). The overall course of these strands resembles the adaxial strands in gerbera, except that the gerbera strands are distinct from the floret veins in a manner implying monopodial

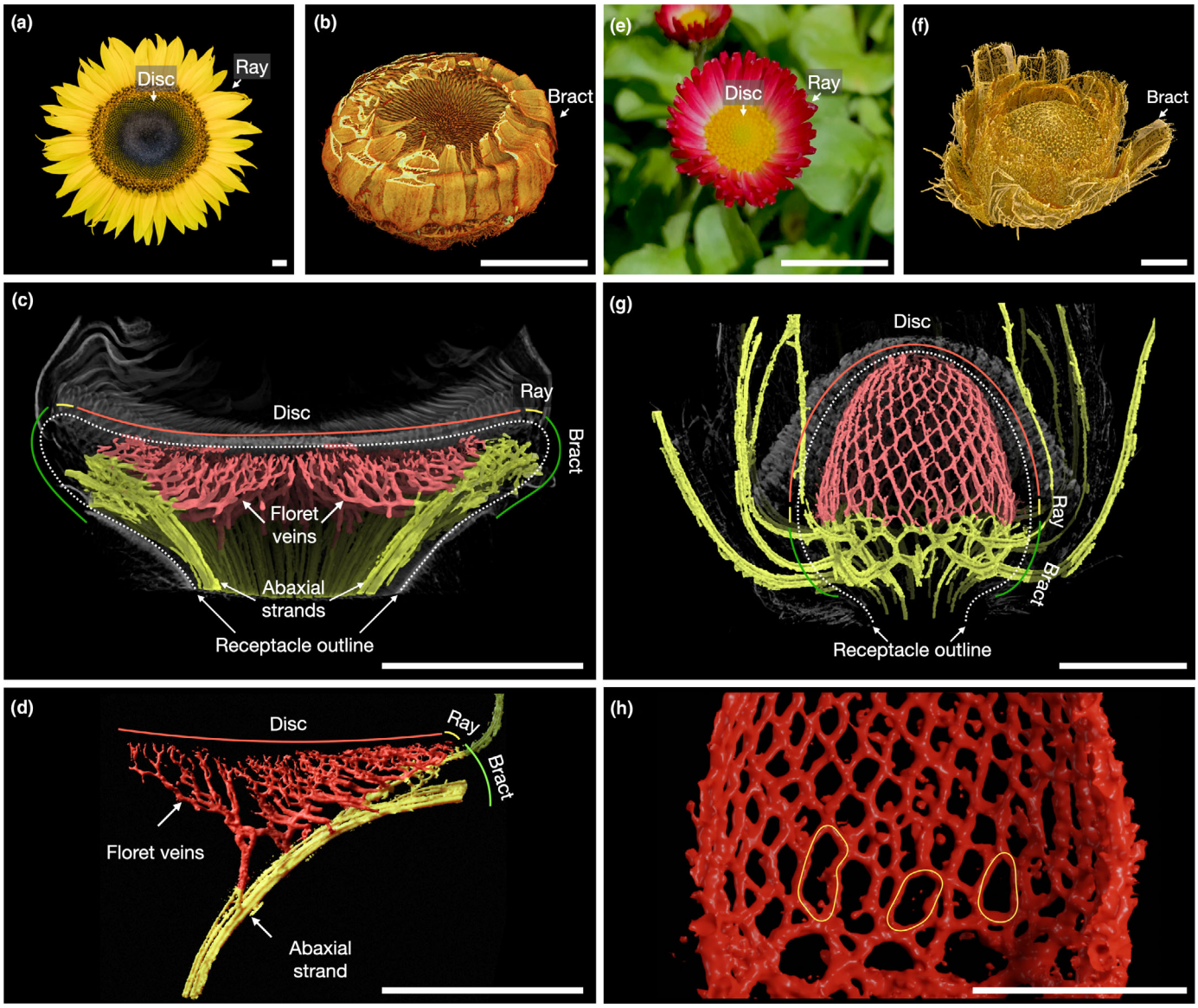

Fig. 3 Vascular systems of sunflower (a–d) and Bellis (e–h) heads. (a) A mature flower head of sunflower bearing two different types of florets: ray and disc. (b) 3D-reconstruction of an earlier developmental stage of a sunflower head. (c) Longitudinal view of half of a sunflower head with the vascular system segmented with SHVR. (d) VINE segmentation showing floret veins connecting to a single abaxial strand in the sunflower head. (e–g) Images of the Bellis head corresponding to (a–c). (h) A magnified view of the reticulate Bellis head venation, highlighting gaps near the base of the vascular system (yellow lines). Bars: (a–c, e) 1 cm; (d) 5 mm; (f–h) 2 mm.

branching, whereas in coneflower, this distinction is absent, implying sympodial branching. Abaxial veins in the coneflower form a reticulate network (Fig. S4c, bottom) similar to that found near the base of Bellis heads.

The receptacle of Tanacetum (Fig. 4g) is more elongated (Fig. 4h,i) than that of coneflower or thistle. The vasculature combines features of a sectorial system, with thick strands running approximately in the radial direction, and reticulation manifest in interconnections between these strands (Figs 4i, S4d). In contrast to thistle and coneflower, these interconnections appear not only in the abaxial strands, but also in the adaxial strands. In contrast to Bellis, the resulting network is not related to the parastichies.

We also investigated two species with globular receptacles and heads representing syncephalia, that is compound structures in which entire heads develop within a head (Zhang & Elomaa, 2021). In Craspedia (Fig. 4j–l), the primary receptacle supports secondary heads with 8–10 florets (Bremer, 1994), whereas in Echinops (Fig. 4m–o), the primary receptacle supports second-order heads composed of a single floret subtended by a bract. In both cases, the vascular strands from the stem attach directly to the marginal secondary heads, as the first-order heads lack involucral bracts. The (primary) vascular system of Craspedia is reticulated in a manner resembling Bellis, although it is less regular and vertically more stretched (Fig. S4e). Due to a

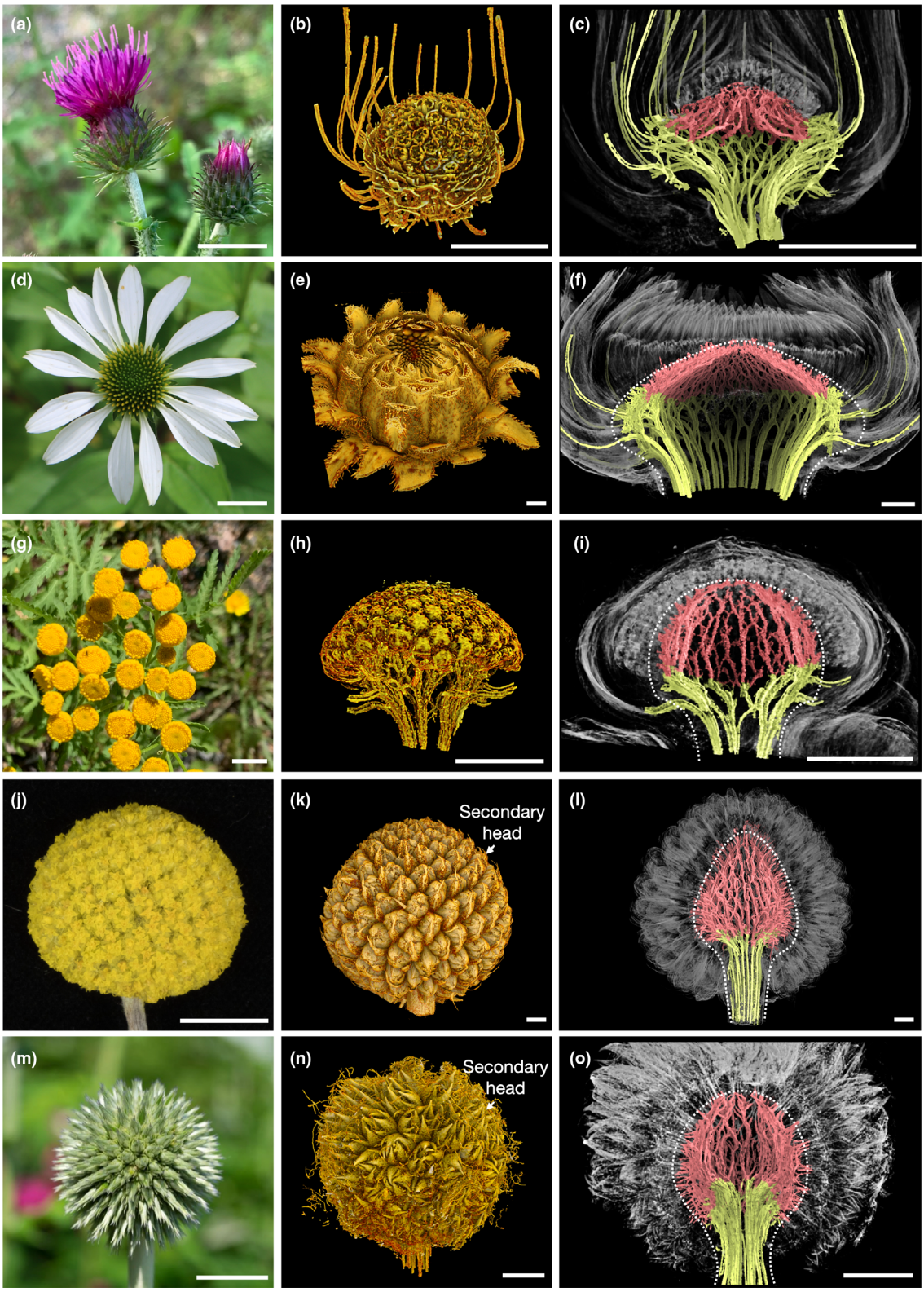

Fig. 4 Vascular architecture in: (a–c) thistle, (d–f) coneflower, (g–i) Tanacetum, (j–l) Craspedia and (m–o) Echinops. The first two columns represent mature inflorescences and 3D reconstructions of flower heads that are fully patterned with primordia. The third column shows longitudinal views of half of the respective flower heads with the vascular system segmented using SHVR. In the case of Craspedia and Echinops, the primary heads support secondary heads rather than individual primordia. Bars: 1 cm in the first column; 1 mm in the second and third columns.

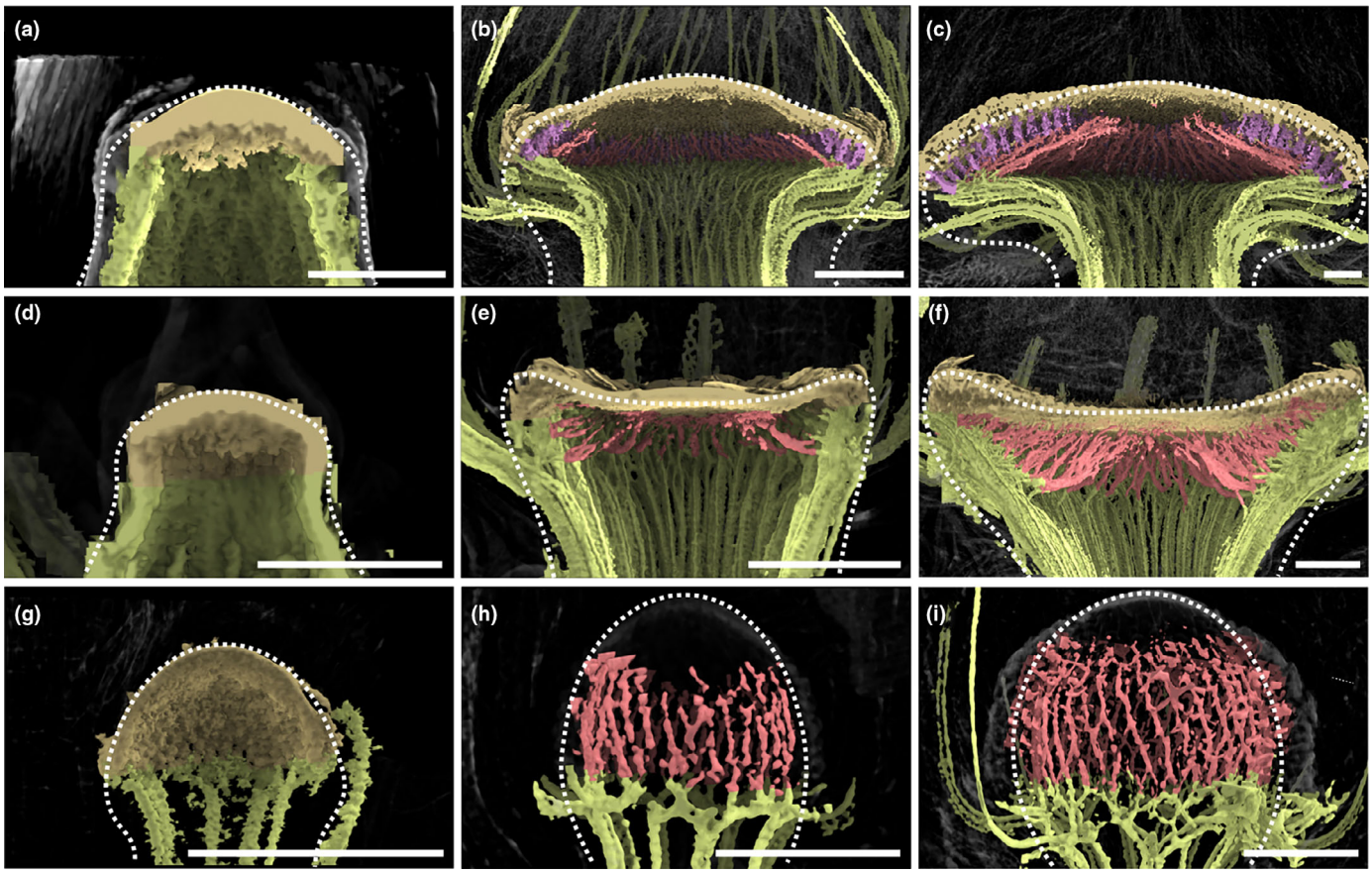

Fig. 5 Ontogeny of the vascular systems at different stages of head development in gerbera (a–c), sunflower (d–f) and Bellis (g–i). The receptacle outlines are marked in dashed white lines. Bars, 0.5 mm.

relatively small number of secondary heads, the vascular system in Echinops is simpler, with the main strands meandering as in Tanacetum and occasionally interconnecting as in Craspedia (Fig. S4f).

The ontogeny of the vascular system correlates with receptacle growth

As a further step toward understanding the development of vascular systems, we observed the head development of gerbera, sunflower, and Bellis over time (Fig. 5). At an early developmental stage, right after the reproductive transition, the receptacles in all three species are dome-shaped. The stem strands are already visible and connect directly to the early bract primordia (Fig. 5a,d,g). As development continues, both the florets that gradually fill the meristem surface and the vascular system that supports them progress from the periphery to the receptacle center (Fig. 5b,e,h). At this stage, the development in the three head types diverge. The gerbera receptacle gradually assumes a convex mushroom shape. This transformation spreads the distal parts of the stem strands outward, producing radially oriented abaxial strands. The tips of the innermost strands turn toward the center of the receptacle, producing adaxial strands (Fig. 5b,c). Short floret veins then connect the emerging florets to the adaxial strands (Fig. 5c). To examine this process further, we analyzed the scans of a transgenic gerbera line, in which the center of the inflorescence meristem remains undifferentiated and does not initiate new floret primordia due to downregulation of *SEPALLATA*-like *GRCD* genes (Uimari *et al.*, 2004; Zhang *et al.*, 2017; Fig. S5). Both the abaxial stem veins and the adaxial veins in these transgenic plants develop as in wild-type gerbera. However, in the head center, the adaxial veins continue to develop toward the center despite of the absence of the floret primordia, and eventually they merge below the undifferentiated meristematic surface closing the network (Fig. S5b,c). Altogether, our data suggest that the centripetal veins in gerbera act as leading strands, to which the veins originating in the florets eventually connect.

In contrast to gerbera, the sunflower heads gradually assume a concave shape (Fig. 5). As florets are patterned in progression toward the center, they become directly connected to the large vascular strands from the stem (Fig. 5e,f). And a still different developmental progression arises in the globular heads of Bellis. Their vascular strands form a reticulate structure aligned with two intersecting families of parastichies. During development, the strands aligned with one family become visible first (Fig. 5h), and the intersecting strands following the opposite family emerge later (Fig. 5i), eventually producing the reticulate pattern (Fig. 3g).

Phyllotactic patterning precedes vascular development in gerbera

Volumetric imaging reveals that organ primordia and vascular strands are already present in the early developmental stages of head development (Figs 5a,d,g, S6). To further explore the association between vascular patterning and phyllotaxis, we examined a transgenic gerbera line expressing the *DR5rev:3xVENUS-N7* auxin reporter (Zhang *et al.*, 2021). Using this line, we first identified the number of auxin maxima on the meristem surface, then performed serial sectioning and histological staining of the same meristem samples (Fig. 6; an example of serial section for histological analysis, corresponding to Fig. 6c, is shown in Fig. S7). In the earliest developmental stage, the first three DR5 maxima (corresponding to future bract primordia) were patterned (Fig. 6a,e). Histological analysis of the sample showed a continuous ring of densely stained cells at the base of the meristem (Fig. 6i). This region represents the procambial or meristematic ring initiating new vascular strands (Esau, 1954). Subsequently, new DR5 maxima emerged, while the procambial region became separated into discrete vascular strands (Fig. 6b–d,f,g,j–l). Their number increased as the head grew, indicating that the new strands were inserted intercalarily between the existing ones (Fig. 6i–l). The number of differentiated vascular strands was always smaller than the number of auxin maxima on the meristem surface, demonstrating that auxin patterning on the surface occurs before the differentiation of vascular strands beneath it. A re-analysis of the live-imaging data of gerbera head meristem from Zhang *et al.* (2021) has further shown that the DR5 signals emerge first on the meristem surface, then gradually extend toward the inner tissues (Fig. S8). Taken together, these observations indicate that the specification of vasculature in gerbera, and likely also in other flower heads, shares a conserved auxin-driven patterning mechanism with other species (Bayer *et al.*, 2009; O'Connor *et al.*, 2014).

A common model captures vascular pattern development in diverse flower heads

The complexity and diversity of vascular patterns in flower heads lead to the question of the underlying developmental mechanism. To identify a plausible candidate, we explored several hypotheses using a computational model (for details, see Methods S2: Supplemental Model Description and the model code referenced in the Data availability section). The model operates on a dynamic template of receptacle growth, simulated using previous data for gerbera (Zhang *et al.*, 2021) and new data for sunflower and Bellis (Fig. S9). The input data also include simulated dynamic patterns of primordia emergence. For gerbera, it is the pattern described by Zhang *et al.* (2021) (Fig. S9c). For the sunflower and Bellis, the phyllotactic patterns have been simulated using the same algorithm, with parameters modified to capture the characteristics of each species (Fig. S9f,i).

Consistent with the observations (Fig. 5), simulations of vascular pattern development proceed through two phases. In the first phase, the emerging vascular strands connect the early primordia (which may develop into involucral bracts) to the procambial ring positioned at the base of the young head. In the second phase, vascular strands originating from the floret primordia veins connect to the previously formed strands. As the head grows, all strands elongate and deform to accommodate the changes in size and shape of the growing receptacle.

We began with the highly regular pattern observed in Bellis heads. The pattern consists of two families of vascular strands aligned with left- and right-winding parastichies (Fig. 3g). These families are not equivalent: The steeper strands are more pronounced and develop before the strands following parastichies running in the opposite direction (Fig. 5h,i). The question thus arises, on what basis the patterning process distinguishes these strands. The simplest hypothesis is that each incipient primordium connects first to the closest point on a previously formed strand. With primordia arranged into a spiral phyllotactic pattern, this point coincides with, or lies near, the closest preceding primordium. However, as the distance of the incipient primordium to its closest neighbors along either contact parastichy is approximately the same, the resulting algorithm produces irregular strands, which reflect inconsistent choices of the parastichy to follow (Fig. S10a).

Seeking an alternative, we hypothesized that each new connection minimizes the resistance to auxin transport from the auxin source located at the incipient primordium to the sink located at the receptacle base. A similar model has been proposed for leaf vasculature (Runions *et al.*, 2017). The paths of emerging connections then depend not only on distances but also on the resistivities (resistances per unit distance) of the undifferentiated ground tissue and the already formed strands. If the resistivity of the ground tissue is high compared with that of the strands, the patterning process will produce the shortest connection between the incipient primordium and the existing vasculature, as the simple distance-minimizing algorithm would. However, if the discrepancy between the resistivities of the ground tissue and newly patterned strands is smaller and both decrease over time, the connections form according to the least resistance criterion and the threads align with a single family of parastichies, for appropriately chosen parameter values (Fig. S10b). An opposite set of parastichies can then be generated by applying, after some delay, the same resistance-minimizing algorithm, but excluding connections running close to those already formed (Fig. S10c). The resulting process reproduces the development and final structure of the reticulate vascular network characteristic of Bellis heads (compare Fig. 7 to Figs 5g–i and 3g; see also Videos S2, S3).

Even in the highly regular vascular pattern of Bellis, some connections needed for 'perfect' reticulation are missing (Fig. 3h). This phenomenon suggests that the secondary connections are formed with some probabilities, rather than deterministically. Moreover, in previous conceptual and computational models of vascular patterning, it has often been postulated that the ground tissue may be polarized, biasing the formation of vascular strands in certain directions (e.g. Sachs, 1991; Bayer *et al.*, 2009). In terms of our model, such bias can be captured by assuming that the resistivity of the ground tissue depends on directions, that is

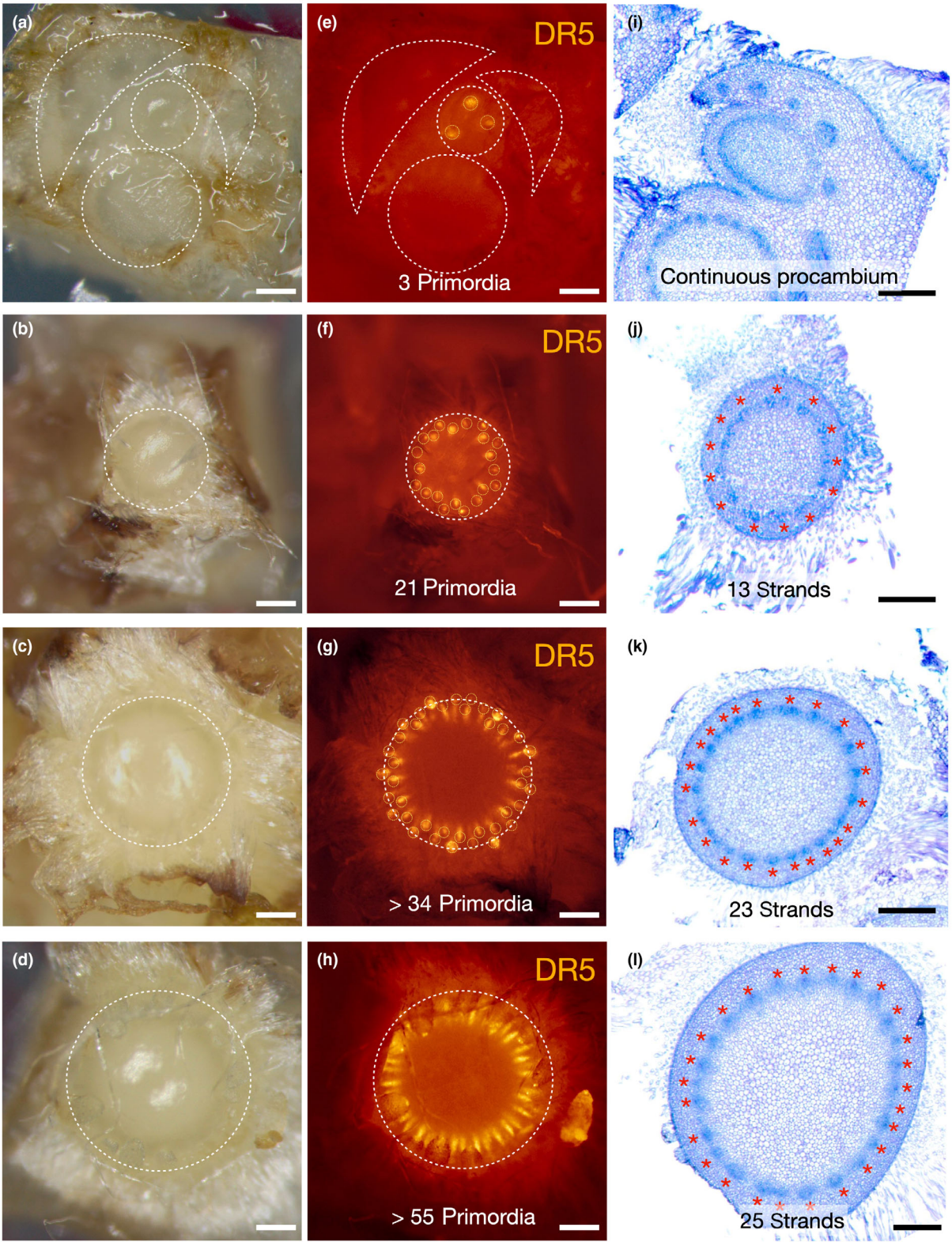

Fig. 6 Association of auxin patterning with patterning of the vasculature. Four independent head meristem samples (a–d) from transgenic gerbera lines expressing the *DR5rev:3xVENUS-N7* auxin reporter (Zhang *et al*., 2021) show increasing numbers of DR5 maxima on the meristem surface corresponding to the emerging bract and floret primordia (e–h). The rightmost column (i–l) shows a representative histological, toluidine blue stained section underneath the surface of the same meristem, with vascular bundles counted and marked with asterisks. Bars, 200 μm.

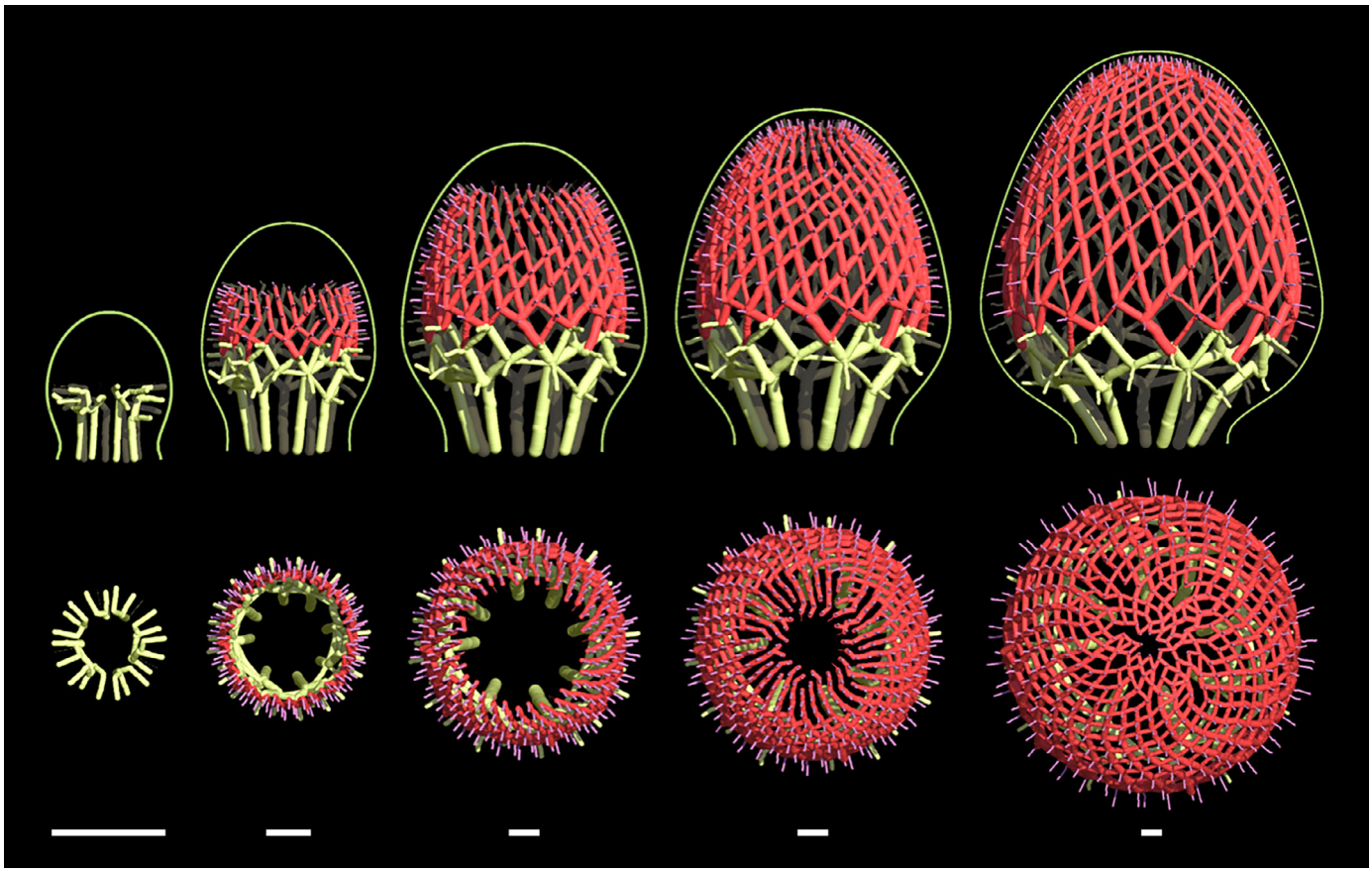

Fig. 7 Simulated development of the Bellis head vasculature. Colors indicate abaxial strands (yellow-green), adaxial strands (red), and floret veins (purple). Scale bars indicate approximately 200 μm.

it is anisotropic. The theoretical morphospace (McGhee, 1999) of structures generated with different probabilities of secondary connections and different degrees of anisotropy on the Bellis head template (Fig. S11) includes patterns approximating the vasculature of the coneflower (Figs 4f, S4c), Tanacetum (Figs 4i, S4d), Craspedia (Figs 4l, S4e), and Echinops (Figs 4o, S4f) heads.

Depending on the head geometry and resistivity values, the paths of least resistance need not run close to the adaxial head surface but may penetrate the ground tissue more deeply, connecting directly to the abaxial strands (Fig. S12a–d). Such paths approximate the vasculature observed in the sunflower (Figs 3a–d, 5e,f) and thistle (Fig. 4c) heads. To model the observed irregular paths of individual strands in the sunflower (Fig. 8; Videos S4–S6), we assumed that the direction in which subsequent segments are added is subject to significant random variation. In addition to the irregularities, the random variation of path extensions promotes the merging of adjacent paths, yielding the highly branched vascular patterns observed in real heads (Fig. S12e,f).

In the cases discussed so far, the development of the vascular system was driven by the emergence of primordia. However, the polarization of ground tissue introduces a reference direction, in which adaxial strands may form ahead of the florets and thus independently of them. The underlying biological mechanism may involve a diffuse region of elevated auxin concentration similar to that observed in the shoot apical meristems of Arabidopsis (Barbier de Reuille *et al.*, 2006; Galvan-Ampudia *et al.*, 2020) toward which the adaxial strands extend. The minimum resistance algorithm then connects floret veins to the nearby adaxial strands, irrespective of the phyllotactic pattern. The resulting vasculature is characteristic of gerbera (compare Figs 9 and 5a–c; see also Videos S7–S9).

Discussion

We have applied laboratory- and synchrotron-radiation-based micro-CT to explore vascular systems of flower heads. The throughput and resolution of micro-CT as well as the ease of sample preparation open the door to the effective screening of vascular structures in plants at different developmental stages. To analyze and segment the complex vascular structures in heads, we developed two interactive programs. SHVR (Gu, 2022) augments images on a standard two-dimensional monitor with tactile feedback, giving the user the impression of touching individual vascular strands. ViNE (Hart, 2020) applies virtual reality technology to view and analyze structures directly in 3D. Both systems allow for relatively fast segmentation, annotation, and interpretation of the heads (*c.* 2 h per sample). Compared with the current AI-assisted segmentation methods, which may automatize the analysis of

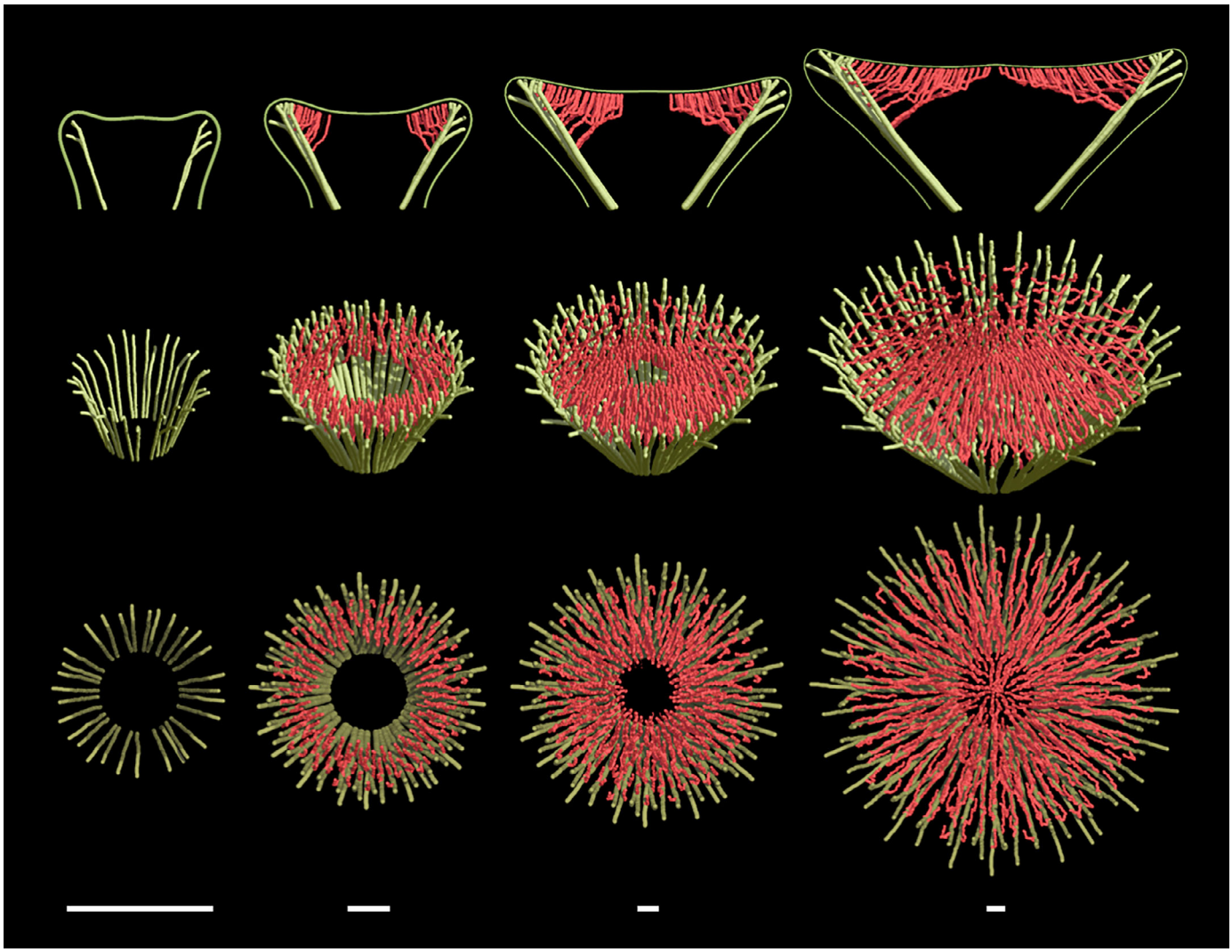

Fig. 8 Simulated development of the sunflower head vasculature. Colors distinguish abaxial strands (yellow-green) from those originating in the florets (red). Scale bars indicate approximately 800 μm.

multiple samples of similar type, but require time-consuming prior training, our systems appear particularly suitable for exploring individual samples of 3D image data.

Our results are summarized in Fig. 10. Using SR-μCT, we have confirmed previous observations of two distinct types of vascular patterns in heads: the reticulate pattern aligned with parastichies exemplified by Bellis (Philipson, 1946) and the sectorial pattern found in sunflower (Durrieu *et al.*, 1985). In the latter case, strands originating in nearby florets form sympodial branching structures that deeply penetrate the ground tissue and connect directly to the abaxial strands. A similar pattern is characteristic of thistle heads. Nevertheless, most observed vascular patterns were shallow, running close to the receptacle surface. Among the heads we have examined, the coneflower was the clearest shallow counterpart of the sunflower, with the sympodial branching structures originating in the florets and connecting to the abaxial veins near the head perimeter. Craspedia, Echinops, and Tanacetum heads combined features of shallow sectorial and reticulate patterns: the course of vascular strands was biased sectorially to some extent, while the patterns included loops, although not as regular as in Bellis. A relative outlier was the sectorial pattern of gerbera, characterized by the presence of radially oriented adaxial strands, to which floret veins connect in a monopodial branching pattern.

To obtain insight into the developmental mechanisms that may produce the observed patterns, we constructed a dynamic model of vascular patterning in flower heads expressed in geometric terms (Owens *et al.*, 2016; Cieslak *et al.*, 2021). A key explicit assumption was that the vascular strands supporting new primordia extend the network formed so far in a manner minimizing the resistance of the resulting paths to the transport of auxin (Runions *et al.*, 2017). To explain the vascular pattern in gerbera, we additionally assumed the presence of a region that attracts the emerging vascular strands, located in the central zone of the apex. With different, time-dependent resistivities of the vascular and ground tissues, our model reproduced the vascular patterns of all observed heads.

Fig. 9 Simulated development of the gerbera head vasculature. Colors distinguish abaxial strands (yellow-green), adaxial strands (red), and floret veins (purple). Disc florets and floret veins have been suppressed in the bottom row to expose adaxial strands. Scale bars indicate approximately 500 μm.

The eight sample species analyzed in this paper are but a minute fraction of the estimated 25 000–35 000 Asteraceae species (Mandel *et al.*, 2019). This disparity leads to the question of whether there are further types of vascular patterns in heads fundamentally different from those encompassed by our study (Fig. 10). If the diversity of vascular patterns in heads echoes that of vein patterns in leaves, we should expect more patterns, even within the confines of our resistance-based model. For instance, our model can readily generate a non-reticulate pattern aligned with a single family of parastichies (Fig. S10b), or a pattern in which each floret connects directly to the base of the head though its own vascular strand (resulting in a vascular structure that resembles the branching architecture of an umbel inflorescence). The efficiency of micro-CT opens the door to addressing the question of vascular pattern diversity through a broad screening of heads.

The diversity of the vascular structures in heads raises the question of the molecular implementation of the patterning mechanism. According to current understanding, vascular patterns in plants result from a feedback mechanism in which auxin regulates its own transport. In this process, maxima of auxin concentration emerge in the epidermis and initiate auxin flow into the subepidermal tissues. There, the flow canalizes into narrow paths that connect to the pre-existing vasculature, patterning new vascular strands (Jacobs, 1952; Sachs, 1969, 1991; Reinhardt *et al.*, 2003; Kang & Dengler, 2004; Scarpella *et al.*, 2006; Wenzel *et al.*, 2007; Bayer *et al.*, 2009; O'Connor *et al.*, 2014). The auxin reporter lines of gerbera indicate that auxin defines the sites of primordia in heads as it does in other model species (Zhang *et al.*, 2021; Fig. S8), which suggests that the course of vascular strands in heads is patterned by a similar mechanism as well. Nevertheless, a more comprehensive analysis of the patterning of vasculature in heads at the molecular level is needed. The crucial next step will be the construction and analysis of transgenic Asteraceae plants reporting the spatio-temporal expression and cell-level distribution of auxin efflux carriers, the PIN1 proteins.

The prevalent view is that phyllotactic patterning of primordia takes place first, guiding the subsequent creation of vascular patterns (Reinhardt *et al.*, 2003; Stoma *et al.*, 2008; Bayer *et al.*, 2009; Kierzkowski *et al.*, 2013; O'Connor *et al.*, 2014). This view is also implicit in the molecular level descriptions of phyllotaxis (e.g. Shi & Vernoux, 2019) and in computational models that generate phyllotactic patterns without involving vasculature (e.g. Jönsson *et al.*, 2006; Smith *et al.*, 2006; Zhang *et al.*, 2021). Nevertheless, an opposite possibility has been

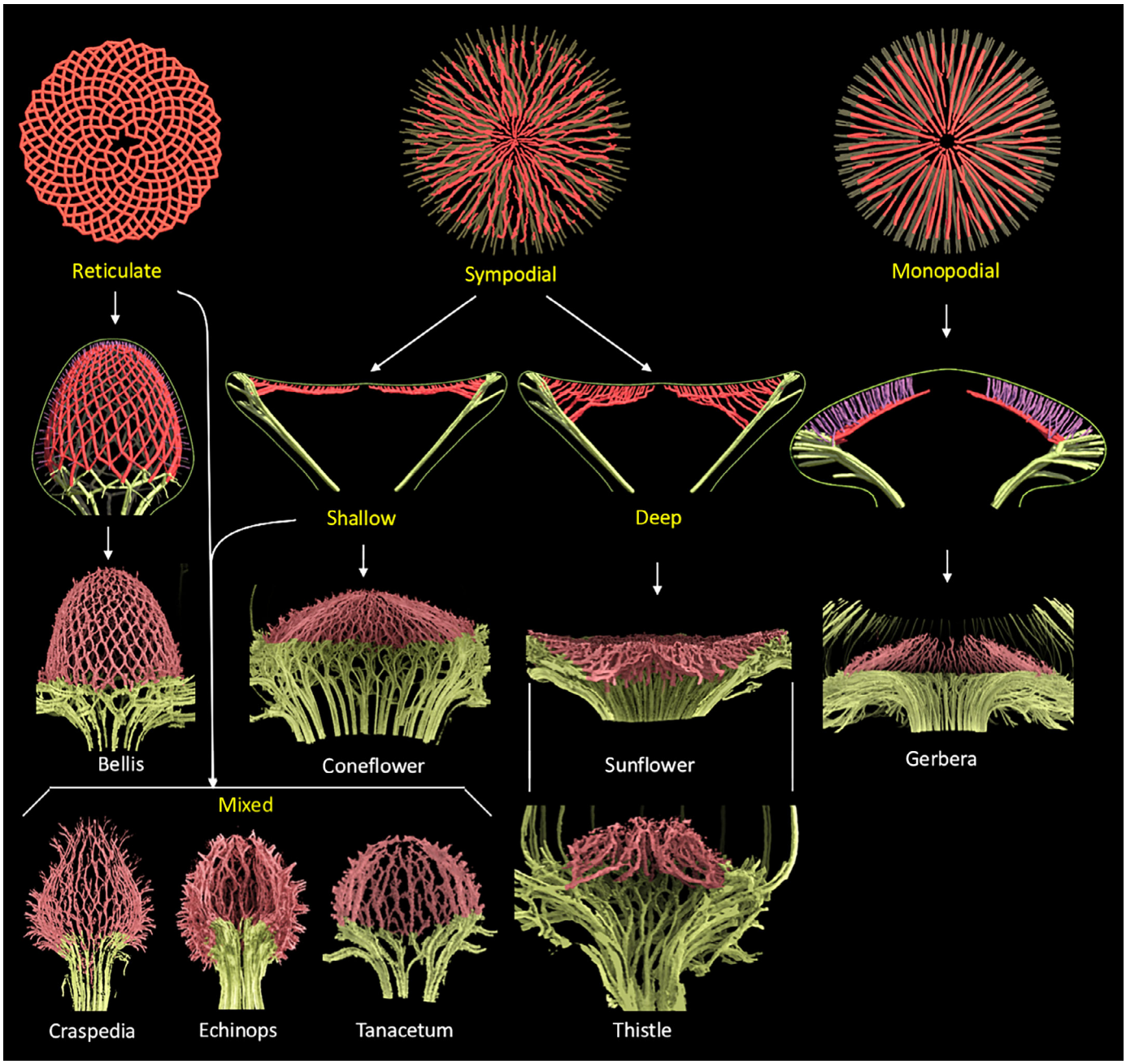

Fig. 10 Comparative analysis of vascular structures in the studied heads. Upper rows: archetype models of the observed vascular structures (top and side views). Reticulate structures have intersecting families of strands, which follow the spiral phyllotactic arrangement of the florets. Sympodial and monopodial structures have strands organized sectorially into sympodial or monopodial branching patterns. The sympodial patterns may remain close to the receptacle surface (shallow patterns) or penetrate the ground tissue (deep patterns). Bottom rows: position of the observed heads with respect to the archetypes. Bellis shows a highly regular reticulate pattern aligned with the spiral arrangement of florets. Sunflower, thistle and coneflower form sympodial branching structures with floret veins connecting to stem veins via deep or shallow sectorial patterns. Vascular systems in Craspedia, Echinops and Tanacetum combine elements of reticulate and shallow sectorial patterns. The vasculature in gerbera differs from other observed species by developing distinct, radial adaxial veins to which floret veins connect in a monopodial pattern.

repetitively raised, suggesting that patterning information flows from the differentiated internal tissues toward the meristem surface and determines or influences organ positioning (Esau, 1954; Larson, 1975; Kang *et al.*, 2003; Banasiak & Zagórska-Marek, 2006; Dengler, 2006; Kuhlemeier, 2007; Korn, 2008; Banasiak, 2011; Aulenback, 2021; Banasiak & Gola, 2023). It is difficult to imagine, however, how the development of highly regular phyllotactic patterns could be driven by locally irregular vascular strands. Likewise, it is not clear how the diversity of vascular patterns could lead to the uniformity of spiral phyllotactic patterns. By contrast, our models show that the observed vascular patterns, with large-scale organization but also with many local

irregularities, can readily arise from regular phyllotactic patterns. Our observations and model thus support the prevalent view of the primacy of phyllotaxis over vascular patterning, although we cannot preclude a causality-blurring feedback mechanism that patterns primordia and vascular strands concurrently. [Correction added on 17 April 2024, after first online publication: edit made to wording in preceding sentence for clarification.]

The relation between the arrangement of florets and the underlying vascular pattern bears upon the long-standing question of the evolutionary origin of flower heads and their diverse vascular patterns. Based on morphological studies of basal relatives of Asteraceae (Menyanthaceae, Goodeniaceae, and Calyceraceae), Pozner *et al.* (2012) suggested that the head-like structures in Calyceraceae and Asteraceae have evolved from branched inflorescences by the gradual reduction to a compact raceme. Considering the vascular system as a vestige of an ancestral free-standing branching system is consistent with our results. Gerbera, which appeared early in the evolution of Asteraceae (Bremer, 1994; Mandel *et al.*, 2019), has heads with adaxial strands to which floret veins attach in a monopodial fashion characteristic of racemes. The patterns we observed in other, evolutionary later species could result from the reduction of these adaxial veins, causing a transition from monopodial to sympodial architecture. This switch could further lead to the alignment of vascular strands with parastichies, following a quantitative reduction of the sectorial bias. We are not certain, however, how much insight the branching architecture of presumed ancestral inflorescences has to offer. As previous work (Harder & Prusinkiewicz, 2013) and our results here show, both architectures may significantly vary without fundamentally affecting the arrangement of the flowers they support. Architectural transformations may therefore be incidental to the central question of how the shoot apical meristem evolved into a receptacle large enough to accommodate hundreds of florets arranged into stereotypical spiral phyllotactic patterns.

Acknowledgements

We thank Dr Heikki Suhonen from the Department of Physics, University of Helsinki, for assistance with laboratory-based micro-CT, Chithra Karunakaran for the suggestion of using SR-μCT for analyzing vascular patterns in plants and early guidance, and the staff at the Biomedical Imaging and Therapy facility at the Canadian Light Source for assistance (the Canadian Light Source, a national research facility of the University of Saskatchewan, is supported by the Canada Foundation for Innovation (CFI), the Natural Sciences and Engineering Research Council (NSERC), the National Research Council (NRC), the Canadian Institutes of Health Research (CIHR), the Government of Saskatchewan, and the University of Saskatchewan). We also thank Sonny Chan for the introduction to haptics and help initiating the SHVR project, Usman Alim for sharing his expertise in volumetric rendering and segmentation, and Lynn Mercer for her work on Methods S2: Supplemental Model Description. This work was supported by the Plant Phenotyping and Imaging Research Centre/Canada First Research Excellence Fund (PP and MC), Academy of Finland Grants 310318 and 341774 (PE), and Natural Sciences and Engineering Research Council of Canada Discovery Grants 2014-05325 and 2019-06279 (PP). We also gratefully acknowledge the support of NVIDIA Corp. with the donation of two GPUs used in this research.

Competing interests

None declared.

Author contributions

PE, PP, TZ and AO designed the research. TZ carried out experimental work and prepared all samples. TZ, JS, MC, PG, AO, PE and PP scanned samples. TZ, MC and JS reconstructed the data stacks. AO, PG and JH wrote the visualization software. TZ, PG, JH, AO and MC visualized the data. AO and MC developed the models. PP, PE, AO, TZ and MC wrote the paper with input from coauthors. MC and TZ curated the data. AO and TZ are joint first authors for this work.

ORCID

Mikolaj Cieslak https://orcid.org/0000-0003-2138-6865
Paula Elomaa https://orcid.org/0000-0001-6512-0810
Philmo Gu https://orcid.org/0009-0001-8008-910X
Jeremy Hart https://orcid.org/0009-0005-8714-1790
Andrew Owens https://orcid.org/0000-0003-1935-8232
Przemyslaw Prusinkiewicz https://orcid.org/0000-0002-1338-7086
Jarvis Stobbs https://orcid.org/0000-0003-0971-2744
Teng Zhang https://orcid.org/0000-0002-5189-3289

Data availability

The reconstructed image stacks, segmentation masks, and polygon meshes (150 GB in total) reported in this paper are openly available at the EMBL-EBI BioImage Archive (https://www.ebi.ac.uk/biostudies/bioimages/studies/S-BIAD1021). The data are organized according to the order of appearance in the figures, as presented in Table S1. Image stacks are saved as multi-page TIF files, with segmentation information in MASK files specific to SHVR. Polygon meshes are in the PLY format, with segmentation information in CLR files specific to ViNE. In addition, a smaller set of down-sampled data for the eight species in our study (3.14 GB in total) is available at the X-plant site: https://www.biw.kuleuven.be/biosyst/mebios/downloads/3d-x-ray-images-of-plant-organs. The Bellis, sunflower and gerbera head vasculature models can be downloaded from http://algorithmicbotany.org/papers/vasculature2024.html or https://github.com/AlgorithmicBotany.

References

Adler I, Barabé D, Jean RV. 1997. A history of the study of phyllotaxis. *Annals of Botany* **80**: 231–244.

Alkio M, Diepenbrock W, Grimm E. 2002. Evidence for sectorial photoassimilate supply in the capitulum of sunflower (*Helianthus annuus*). *New Phytologist* **156**: 445–456.

Aulenback KR. 2021. *Stelar evolution and morphology in selected taxa based on vasculotaxy*. Self-published.
Banasiak A. 2011. Putative dual pathway of auxin transport in organogenesis of *Arabidopsis*. *Planta* **233**: 49–61.
Banasiak A, Gola EM. 2023. Organ patterning at the shoot apical meristem (SAM): the potential role of the vascular system. *Symmetry* **15**: 364.
Banasiak A, Zagórska-Marek B. 2006. Signals flowing from mature tissues to shoot apical meristem affect phyllotaxis in coniferous shoot. *Acta Societatis Botanicorum Poloniae* **75**: 113–121.
Barabé D, Lacroix C. 2020. *Phyllotactic patterns: a multidisciplinary approach*. Singapore City, Singapore: World Scientific.
Barbier de Reuille P, Bohn-Courseau I, Ljung K, Morin H, Carraro N, Godin C, Traas J. 2006. Computer simulations reveal properties of the cell-cell signaling network at the shoot apex in *Arabidopsis*. *Proceedings of the National Academy of Sciences, USA* **103**: 1627–1632.
Barbier de Reuille P, Routier-Kierzkowska A-L, Kierzkowski D, Bassel GW, Schüpbach T, Tauriello G, Bajpai N, Strauss S, Weber A, Kiss A *et al.* 2015. MorphographX: a platform for quantifying morphogenesis in 4D. *eLife* **4**: e05864.
Bayer EM, Smith RS, Mandel T, Nakayama N, Sauer M, Prusinkiewicz P, Kuhlemeier C. 2009. Integration of transport-based models for phyllotaxis and midvein formation. *Genes and Development* **23**: 373–384.
Bremer K. 1994. *Asteraceae, cladistics and classification*. Portland, OR, USA: Timber Press.
Brodersen CR, Lee EF, Choat B, Jansen S, Phillips RJ, Shackel KA, McElrone AJ, Matthews MA. 2011. Automated analysis of three-dimensional xylem networks using high-resolution computed tomography. *New Phytologist* **191**: 1168–1179.
Brodersen CR, Roark LC, Pittermann J. 2012. The physiological implications of primary xylem organization in two ferns. *Plant, Cell & Environment* **35**: 1898–1911.
Brodersen CR, Roddy AB. 2016. New frontiers in the three-dimensional visualization of plant structure and function. *American Journal of Botany* **103**: 184–188.
Cieslak M, Owens A, Prusinkiewicz P. 2021. Computational models of auxin-driven patterning in shoots. *Cold Spring Harbor Perspectives in Biology* **14**: a040097.
Dengler NG. 2006. The shoot apical meristem and development of vascular architecture. *Canadian Journal of Botany* **84**: 1660–1671.
Dhondt S, Vanhaeren H, Van Loo D, Cnudde V, Inzé D. 2010. Plant structure visualization by high-resolution X-ray computed tomography. *Trends in Plant Science* **15**: 419–422.
Durrieu G, Percie du Sert C, Merrien A. 1985. Anatomie du capitule de tournesol consequences sur la nutrition des akenes. In: *Proceedings of XI International Sunflower Conference*. Buenos Aires, Argentina: Association Argentina de Girasol, Actas Comptes-Rendus Proceedings, 7–12.
Esau K. 1954. Primary vascular differentiation in plants. *Biological Reviews* **29**: 46–86.
Esau K. 1965a. *Plant anatomy*. New York, NY, USA: John Wiley & Sons.
Esau K. 1965b. *Vascular differentiation in plants*. New York, NY, USA: Holt, Rinehart and Winston.
Faragó T, Gasilov S, Emslie I, Zuber M, Helfen L, Vogelgesang M, Baumbach T. 2022. Tofu: a fast, versatile and user-friendly image processing toolkit for computed tomography. *Journal of Synchrotron Radiation* **29**: 916–927.
Galvan-Ampudia CS, Cerutti G, Legrand J, Brunoud G, Martin-Arevalillo R, Azais R, Bayle V, Moussu S, Wenzl C, Jaillais Y *et al.* 2020. Temporal integration of auxin information for the regulation of patterning. *eLife* **9**: e55832.
Gu P. 2022. *Annotation of vascular plant structures using haptic assistance*. MSc Thesis, University of Calgary, Calgary, AB, Canada.
Harder LD, Prusinkiewicz P. 2013. The interplay between inflorescence development and function as the crucible of architectural diversity. *Annals of Botany* **112**: 1477–1493.
Hart J. 2020. *Interactive visualization and modeling of plant structures in virtual reality*. MSc Thesis, University of Calgary, Calgary, AB, Canada.
Jacobs WP. 1952. The role of auxin in differentiation of xylem around a wound. *American Journal of Botany* **39**: 301–309.
Jean R. 1994. *Phyllotaxis: a systemic study in plant morphogenesis*. Cambridge, UK: Cambridge University Press.
Jönsson H, Heisler MG, Shapiro BE, Meyerowitz EM, Mjolsness E. 2006. An auxin-driven polarized transport model for phyllotaxis. *Proceedings of the National Academy of Sciences, USA* **103**: 1633–1638.
Kang J, Dengler N. 2004. Vein pattern development in adult leaves of *Arabidopsis thaliana*. *International Journal of Plant Science* **165**: 231–242.
Kang J, Tang J, Donnelly P, Dengler N. 2003. Primary vascular pattern and expression of *ATHB-8* in shoots of *Arabidopsis*. *New Phytologist* **158**: 443–454.
Kaplan R. 1937. Uber die Bildung der Stele aus dem Urmeristem von Pteridophyten und Spermatophyten. *Planta* **27**: 224–268.
Karunakaran C, Lahlali R, Zhu N, Webb AM, Schmidt M, Fransishyn K, Belev G, Wysokinski T, Olson J, Cooper DM *et al.* 2015. Factors influencing real time internal structural visualization and dynamic process monitoring in plants using synchrotron-based phase contrast X-ray imaging. *Scientific Reports* **5**: 12119.
Karwowski R, Prusinkiewicz P. 2003. Design and implementation of the L+C modeling language. *Electronic Notes in Theoretical Computer Science* **86**: 134–152.
Kierzkowski D, Lenhard M, Smith R, Kuhlemeier C. 2013. Interaction between meristem tissue layers controls phyllotaxis. *Developmental Cell* **26**: 616–628.
Korn RW. 2008. Phyllotaxis: theories and evaluation. *International Journal of Plant Developmental Biology* **2**: 1–12.
Kuhlemeier C. 2007. Phyllotaxis. *Trends in Plant Science* **12**: 1360–1385.
Laitinen R, Broholm S, Albert VA, Teeri TH, Elomaa P. 2006. Patterns of MADS-box gene expression mark flower-type development in *Gerbera hybrida* (Asteraceae). *BMC Plant Biology* **6**: 11.
Larson PR. 1975. Development and organization of the primary vascular system in *Populus deltoides* according to phyllotaxy. *American Journal of Botany* **62**: 1084–1099.
Lee K, Avondo J, Morrison H, Blot L, Stark M, Sharpe J, Bangham A, Coen E. 2006. Visualizing plant development and gene expression in three dimensions using optical projection tomography. *Plant Cell* **18**: 2145–2156.
Lucas WJ, Groover A, Lichtenberger R, Furuta K, Yadav SR, Helariutta Y, He XQ, Fukuda H, Kang J, Brady SM *et al.* 2013. The plant vascular system: evolution, development and functions. *Journal of Integrative Plant Biology* **55**: 294–388.
Mandel J, Dikow RB, Sinscalchi CM, Thapa R, Watson LE, Funk VA. 2019. A fully resolved backbone phylogeny reveals numerous dispersals and explosive diversifications throughout the history of Asteraceae. *Proceedings of the National Academy of Sciences, USA* **116**: 14083–14088.
McElrone AJ, Choat B, Parkinson DY, MacDowell AA, Brodersen CR. 2013. Using high resolution computed tomography to visualize the three dimensional structure and function of plant vasculature. *Journal of Visualized Experiments* **5**: e50162.
McGhee GR. 1999. *Theoretical morphology – the concept and its applications*. New York, NY, USA: Columbia University Press.
O'Connor D, Runions A, Sluis A, Bragg J, Vogel J, Prusinkiewicz P, Hake S. 2014. A division in PIN-mediated auxin patterning during organ initiation in grasses. *PLoS Computational Biology* **10**: e1003447.
Owens A, Cieslak M, Hart J, Classen-Bockhoff R, Prusinkiewicz P. 2016. Modeling dense inflorescences. *ACM Transactions on Graphics* **35**: 136.
Philipson WR. 1946. Studies in the development of the inflorescence I. The capitulum of *Bellis perennis* L. *Annals of Botany* **39**: 257–270.
Philipson WR. 1948. Studies in the development of the inflorescence IV. The capitula of *Hieracium boreale* Fries and *Dahlia gracilis* Ortg. *Annals of Botany* **12**: 65–75.
Piovesan A, Vancauwenberghe V, Van De Looverbosch T, Verboven P, Nicolaï B. 2021. X-ray computed tomography for 3D plant imaging. *Trends in Plant Science* **26**: 1171–1185.
Pozner R, Zanotti C, Johnson LA. 2012. Evolutionary origins of the Asteraceae capitulum: insights from Calyceraceae. *American Journal of Botany* **99**: 1–13.
Prunet N, Duncan K. 2020. Imaging flowers: a guide to current microscopy and tomography techniques to study flower development. *Journal of Experimental Botany* **71**: 2898–2909.
Prusinkiewicz P, Karwowski R, Lane B. 2007. The L+ C plant-modelling language. In: Vos J, Marcelis LFM, de Visser PHB, Struick PC, Evers JB, eds. *Functional-structural plant modeling in crop production*. Dordrecht, the Netherlands: Springer, 27–42.
Prusinkiewicz P, Runions A. 2012. Computational models of plant development and form. *New Phytologist* **193**: 549–569.
Reinhardt D, Pesce E-R, Stieger P, Mandel T, Baltensperger K, Bennett M, Traas J, Friml J, Kuhlemeier C. 2003. Regulation of phyllotaxis by polar auxin transport. *Nature* **432**: 255–260.

Runions A, Smith RS, Prusinkiewicz P. 2014. Computational models of auxin-driven development. In: Zažímalová E, Petrášek J, Benková E, eds. *Auxin and its role in plant development*. Wien, Austria: Springer, 315–357.

Runions A, Tsiantis M, Prusinkiewicz P. 2017. A common developmental program can produce diverse leaf shapes. *New Phytologist* **216**: 401–418.

Sachs T. 1969. Polarity and the induction of organized vascular tissues. *Annals of Botany* **33**: 263–275.

Sachs T. 1991. *Pattern formation in plant tissues*. Cambridge, UK: Cambridge University Press.

Scarpella E, Marcos D, Friml J, Berleth T. 2006. Control of leaf vascular patterning by polar auxin transport. *Genes and Development* **20**: 1015–1027.

Schindelin J, Arganda-Carreras I, Frise E, Kaynig V, Longair M, Pietzsch T, Preibisch S, Rueden C, Saalfeld S, Schmid B *et al.* 2012. Fiji: an open-source platform for biological-image analysis. *Nature Methods* **9**: 676–682.

Shi B, Vernoux T. 2019. Patterning at the shoot apical meristem and phyllotaxis. *Current Topics in Developmental Biology* **131**: 81–107.

Smith RS, Guyomarc'h S, Mandel T, Reinhardt D, Kuhlemeier C, Prusinkiewicz P. 2006. A plausible model of phyllotaxis. *Proceedings of the National Academy of Sciences, USA* **103**: 1301–1306.

Stoma S, Lucas M, Chopard J, Schaedel M, Traas J, Godin C. 2008. Flux-based transport enhancement as a plausible unifying mechanism for auxin transport in meristem development. *PLoS Computational Biology* **4**: 1000207.

Stuppy WH, Maisano JA, Colbert MW, Rudall PJ, Rowe TB. 2003. Three-dimensional analysis of plant structure using high-resolution X-ray computed tomography. *Trends in Plant Science* **8**: 2–6.

Uimari A, Kotilainen M, Elomaa P, Yu D, Albert VA, Teeri TH. 2004. Integration of reproductive meristem fates by a *SEPALLATA*-like MADS-box gene. *Proceedings of the National Academy of Sciences, USA* **101**: 15817–15822.

Vogelgesang M, Faragó T, Morgeneyer TF, Helfen L, dos Santos RT, Myagotin A, Baumbach T. 2016. Real-time image-content-based beamline control for smart 4D X-ray imaging. *Journal of Synchrotron Radiation* **23**: 1254–1263.

Wenzel CL, Schuetz M, Yu Q, Mattsson J. 2007. Dynamics of *MONOPTEROS* and PIN-FORMED1 expression during leaf vein pattern formation in *Arabidopsis thaliana*. *The Plant Journal* **49**: 387–398.

Withers PJ, Bouman C, Carmignato S, Cnudde V, Grimaldi D, Hagen CK, Maire E, Manley M, Du Plessis A, Stock SR. 2021. X-ray computed tomography. *Nature Reviews Methods Primers* **1**: 1–21.

Zhang T, Cieslak M, Owens A, Wang F, Broholm SK, Teeri TH, Elomaa P, Prusinkiewicz P. 2021. Phyllotactic patterning of gerbera flower heads. *Proceedings of the National Academy of Sciences, USA* **118**: e2016304118.

Zhang T, Elomaa P. 2021. Don't be fooled: false flowers in Asteraceae. *Current Opinion in Plant Biology* **59**: 101972.

Zhang T, Zhao Y, Juntheikki I, Mouhu K, Broholm SK, Rijpkema AS, Kins L, Lan T, Albert VA, Teeri TH *et al.* 2017. Dissecting functions of *SEPALLATA*-like MADS box genes in patterning of the pseudanthial inflorescence on *Gerbera hybrida*. *New Phytologist* **216**: 939–954.

Supporting Information

Additional Supporting Information may be found online in the Supporting Information section at the end of the article.

Fig. S1 Volume rendering of a gerbera flower head.

Fig. S2 Relation between primordia and vasculature in a sunflower head.

Fig. S3 Relation between primordia and vasculature in a Bellis flower head.

Fig. S4 Intermediate vascular system in selected flower heads.

Fig. S5 Vascular system in a transgenic gerbera head with a downregulated *GRCD* gene.

Fig. S6 Gerbera head meristem at an early stage of development.

Fig. S7 Example of serial section for histological analysis.

Fig. S8 Auxin distribution in emerging primordia.

Fig. S9 Construction of the head templates.

Fig. S10 Key conceptual steps leading to the model of vascular patterning in Bellis heads.

Fig. S11 Impact of increasing sectoriality and reticulation on simulated vascular patterns.

Fig. S12 Exploration of the parameter space of sympodial vasculature.

Table S1 Tomography, imaging techniques, and datasets.

Methods S1 Details of synchrotron scanning.

Methods S2 Supplemental model description.

Video S1 Fly-through of a scanned and segmented gerbera head.

Video S2 Simulated development of a Bellis head vasculature – side view.

Video S3 Simulated development of a Bellis head vasculature – top view.

Video S4 Simulated development of a sunflower head vasculature – side view.

Video S5 Simulated development of a sunflower head vasculature – high-angle view.

Video S6 Simulated development of a sunflower head vasculature – top view.

Video S7 Simulated development of a gerbera head vasculature – side view.

Video S8 Simulated development of a gerbera head vasculature – high-angle view.

Video S9 Simulated development of a gerbera head vasculature – top view.

Please note: Wiley is not responsible for the content or functionality of any Supporting Information supplied by the authors. Any queries (other than missing material) should be directed to the *New Phytologist* Central Office.